Advances in Geo-Energy Research

Vol. 19, No. 1, p. 1-13, 2026

Original article

Key controlling factors of CO_2 huff and puff in normal-pressure marine shale gas reservoirs and pilot test in the Nanchuan block

Yiyu Lu[1,2], Baixue Wang[1,2], Zhaohui Lu[1,2]*, Dazhi Fang[1,2,3], Weijun Ma[3], Michael Hood[1,2]

[1]*State Key Laboratory of Coal Mine Disaster Dynamics and Control, Chongqing University, Chongqing 400044, P. R. China*

[2]*School of Resources and Safety Engineering, Chongqing University, Chongqing 400044, P. R. China*

[3]*Sinopec East China Oil & Gas Company, Nanjing 210011, P. R. China*

Keywords:
Normal-pressure shale gas
CO_2 huff and puff
competitive adsorption
displacement replacement
CO_2 storage

Cited as:
Lu, Y., Wang, B., Lu, Z., Fang, D., Ma, W., Hood, M. Key controlling factors of CO_2 huff and puff in normal-pressure marine shale gas reservoirs and pilot test in the Nanchuan block. Advances in Geo-Energy Research, 2026, 19(1): 1-13. https://doi.org/10.46690/ager.2026.01.01

Abstract:
As China's dominant shale gas hub, the Sichuan Basin faces declining recovery during late-stage reservoir development. This study uses an integrated approach to investigate the potential of CO_2-enhanced shale gas recovery and geological storage in the normal-pressure marine shale of the Nanchuan block. Isothermal adsorption experiments reveal that the Nanchuan shale exhibits a preferential selectivity for CO_2 over CH_4 and a higher gas adsorption capacity compared to other basins, highlighting its inherent potential for both enhanced recovery and carbon sequestration. Using foundational parameters from core experiments and historical production data, a dual-permeability numerical model is constructed. This model is then validated via history matching, demonstrating strong agreement with China's first CO_2 huff and puff field test in this normal-pressure gas reservoir, achieving a recovery boost of 2.9%. Leveraging this validated model, sensitivity analyses are employed to identify the key controlling parameters, optimizing the CO_2 injection amount to 0.3-0.5 pore volumes at a reservoir pressure depletion of 45%-55%, followed by a shut-in period of 15-60 days. The findings confirm the feasibility of CO_2-enhanced shale gas recovery in Nanchuan shale and provide a robust theoretical and technical basis for practical application.

1. Introduction

Shale gas, as one of the most promising clean and efficient energy sources, plays an increasingly vital role in the global energy supply (Zou et al., 2023). However, during late-stage production, shale gas wells generally exhibit low recovery, typically less than 30% (Zou et al., 2010). Driven by carbon capture, utilization and storage technology, the utilization of greenhouse gases in shale gas development has garnered significant attention. CO_2 enhanced shale gas recovery (CO_2-ESGR) leverages the low density and high viscosity of supercritical CO_2 to efficiently transform the reservoir, displace adsorbed CH_4, and improve recovery while achieving geological carbon storage, which has important economic and environmental significance (Godec et al., 2014; Hamza et al., 2021; Chang et al., 2024). Furthermore, the CO_2-based enhanced recovery approach has been extensively studied and applied in shale oil development (Song et al., 2024; Liu et al., 2025a, 2025b; Yu et al., 2025).

Research on the mechanisms of CO_2-ESGR primarily focuses on three aspects: Eompetitive adsorption, diffusion seepage, and geological storage. Numerical simulation methods have formed a multi-scale research system from molecular dynamics simulation at the molecular scale, the lattice

Yandy Scientific Press

*Corresponding author.
E-mail address: luyiyu@cqu.edu.cn (Y. Lu); 20232001002z@stu.cqu.edu.cn (B. Wang); luzhaohui929@126.com (Z. Lu); fangdz.hdsj@sinopec.com (D. Fang); mawj.hdsj@sinopec.com (W. Ma); mikehood49@me.com (M. Hood).

Received October 9, 2025; revised November 2, 2025; accepted November 19, 2025; available online November 23, 2025.

Boltzmann method at the pore scale, to numerical simulation of reservoirs at the macro scale (Zhang et al., 2020; Tang et al., 2023; Zhang et al., 2024). The matrix-fracture dual pore model has been widely adopted, while the adsorption model mostly adapts the Langmuir or extended Langmuir equation, and the transport model needs to consider the slip effect and non-Darcy flow. Extensive experimental and simulation studies have highlighted that CO_2 generally exhibits an adsorption capacity that is 2-5 times higher compared to CH_4. This difference is mainly due to the larger quadrupole moment and stronger surface interaction of CO_2 molecules (Iddphonce and Wang, 2021; Yang et al., 2021; Liao et al., 2023; Zhao et al., 2024). The adsorption energy of CO_2 is 15-25 kJ/mol lower than that of CH_4, and it is more ready to be adsorbed and replace CH_4 in kerogen nanopores. Gas migration in the shale matrix involves various mechanisms including Knudsen diffusion, surface diffusion, and viscous flow (Du et al., 2017; Du et al., 2019; Xie et al., 2023), where the diffusion coefficient of CO_2 is usually 10%-30% lower than that of CH_4, while the concentration gradient can still drive effective replacement. The mechanisms of CO_2 storage mainly include structural, residual, solubility, and mineral storage (Jia et al., 2022; Zhao et al., 2023; Li et al., 2024). Recent molecular studies continue to provide new insights into the sequestration mechanisms and enhanced recovery potential even under more complex conditions such as in water-bearing shale systems (Yang et al., 2025). Numerous studies have demonstrated that 30% to 55% of injected CO_2 is adsorbed onto the shale matrix pore surfaces, promoting CH_4 desorption and contributing to an additional natural gas recovery of 8% to 16% (Omari et al., 2022). Numerical modeling has quantified the parameter effects (CO_2/CH_4 adsorption capacity ratio, reservoir pressure, injection rate/timing) on CH_4 recovery and CO_2 sequestration, providing operational optimization guidelines (Wang et al., 2025a). In terms of engineering practice, the Chattanooga shale layer was subject to a 510-ton CO_2 huff and puff test (Louk et al., 2017), which confirmed the potential of CO_2-ESGR and CO_2 storage. Godec et al. (2013) studied the enhanced gas recovery and CO_2 sequestration potential of the Marcellus shale and used reservoir simulation to examine the injection effect under varying well spacing. A numerical simulation of a single well in the mid-deep shale gas reservoir in the Sichuan Basin (Liu et al., 2024) showed that higher CO_2 ratio and shut-in time are beneficial to enhancing gas recovery. Compared with gas wells without CO_2 injection, the injection of CO_2 can increase the estimated ultimate recovery (EUR) of a single well by 14.2%-19.8%. The above research on the CO_2 storage mechanism provides a sound theoretical basis for CO_2-ESGR, and relevant engineering practices have also verified the feasibility of this technology (Afari et al., 2023; Wang et al., 2024, 2025b).

The Sichuan Basin hosts a substantial resource of normal-pressure marine shale gas, while a significant volume of adsorbed gas remains trapped within depleted wells, posing a challenge for effective production. CO_2 injection into these wells presents a promising strategy to unlock this resource through competitive adsorption mechanisms, thereby substantially enhancing ultimate recovery. To explore this possibility, China's first CO_2 huff and puff field test in a normal-pressure marine shale gas reservoir was conducted in the Nanchuan block. To this end, this study establishes a systematic workflow in which experimental core data and field production history provide direct inputs for building a representative numerical model. This model, calibrated via history matching, is employed to systematically elucidate the impact of key operational parameters, including CO_2 injection amount, shut-in time, and injection timing. The findings offer a scientific basis for optimizing CO_2-ESGR operations and highlight the potential for revitalizing depleted shale gas assets.

2. Methods

2.1 Key recovery mechanism

Natural gas in shale reservoirs exists in three primary states: Free gas (G_f), adsorbed gas (G_a), and solution gas (G_s). The total gas content (G_t) can be expressed as (Zhou et al., 2023):

$$G_t = G_f + G_a + G_s \tag{1}$$

In depleted shale gas wells, a significant portion of gas remains trapped within the pore-fracture system. CO_2-ESGR aims to unlock this resource by injecting CO_2 to replenish reservoir energy. During the shut-in stage of the huff and puff process, CO_2 penetrates micro-fractures and nanopores, promoting the desorption of shale gas from the adsorbed to the free state. Upon well reopening, this displaced gas flows through the fracture network to the wellbore.

Gas adsorption behavior on shale is typically described by the Langmuir model (Zhan et al., 2021):

$$V = \frac{V_L P}{P_L + P} \tag{2}$$

where V represents the adsorbed gas volume, V_L represents the Langmuir volume, P_L represents the Langmuir pressure, and P is gas pressure.

The stronger adsorption affinity of CO_2 compared to CH_4 enables CO_2 molecules to displace pre-adsorbed CH_4 via competitive adsorption (Duan et al., 2016; Gu et al., 2017; Hu et al., 2019). The competitive adsorption selectivity coefficient α can be defined as (Yang et al., 2015):

$$\alpha = \frac{x_1/x_2}{y_1/y_2} \tag{3}$$

where x_1 and y_1 represent the mole fractions of adsorbed and free CO_2, and x_2 and y_2 are those of CH_4, respectively. Studies have confirmed that the adsorption heat, negative Gibbs free energy change, and negative surface potential of CO_2 on shale are greater than those of CH_4, with α typically exceeding 2.5, underscoring the preferential adsorption of CO_2.

In addition to competitive adsorption, CO_2 injection increases reservoir pressure, enhancing both the adsorption capacity and the storage potential of CO_2. Concurrently, the influx of CO_2 reduces the partial pressure of CH_4, further promoting CH_4 desorption, which is known as the partial pressure reduction effect (Lu et al., 2022).

Mass transfer and diffusion also play crucial roles in gas

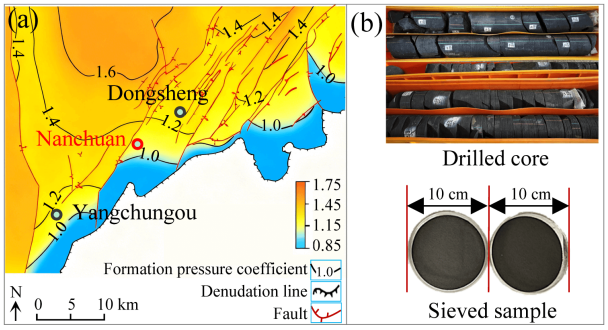

Fig. 1. Research information: (a) Location of the test well and (b) sample preparation.

Table 1. Temperature-pressure variation during well shut-in.

Stage	Wellhead		Bottom hole	
	Pressure (MPa)	Temperature (°C)	Pressure (MPa)	Temperature (°C)
Initial	1.07	23.01	2.05	107.00
Day 2	4.89	14.09	18.71	104.59
Day 8	5.02	17.79	13.29	109.30
Day 14	5.10	20.08	12.51	110.17
Day 17	5.17	20.15	12.53	110.18

recovery (Wang et al., 2012). In the supercritical state (31.1 °C, 7.38 MPa), CO_2 exhibits low viscosity, high diffusivity, strong solubility, and zero surface tension, allowing it to access narrow pores and displace CH_4 (Wang et al., 2012). The desorbed CH_4 is then driven toward production wells by continuous CO_2 convection. Gas migration in shale involves various mechanisms including Darcy flow, Knudsen diffusion, and surface diffusion (Du et al., 2017). The diffusion coefficient D can be modeled as (Du et al., 2019):

$$D = \frac{D_0}{\Phi \cdot \tau \cdot (1 + \mathrm{Kn})} \tag{4}$$

where D_0 represents the free-space diffusion coefficient, Φ represents porosity, τ represents tortuosity, and Kn is the Knudsen number. This model accurately characterizes shale gas diffusion capacity, showing a negative correlation with pressure and a positive correlation with pore diameter.

2.2 Experiments

2.2.1 Materials

Core samples were obtained from a test well in the Pingqiao anticline, Nanchuan block (Fig. 1), with a buried depth interval of 1,810.82-1,888 m. The core sample was mechanically crushed and sieved to obtain 60-80 mesh uniform particles. These were dried at 105 °C constant temperature for 24 hours to completely remove free water and part of the bound water in the sample, to ensure the reliability of subsequent isothermal adsorption and CO_2 displacement CH_4 experiments. This pretreatment strictly followed standard procedures for the shale gas adsorption-desorption experiments.

Table 2. Evaluation parameters of high-quality shale layers in the Longmaxi Formation.

Strata	TOC (%)	Quartz (%)	Clay mineral (%)	Porosity (%)	Gas content (m^3/t)
Longmaxi-layer 5	2.19	40.0	33.8	3.1	2.9
Longmaxi-layer 4	3.53	45.0	21.4	4.9	6.2
Longmaxi-layer 3	4.94	55.0	20.8	5.5	6.9
Longmaxi-layer 2	6.18	62.0	19.6	4.3	8.1
Wufeng-layer 1	4.65	70.0	18.1	5.0	5.5

2.2.2 Experimental system

To investigate shale gas adsorption and displacement characteristics, an integrated experimental system was employed (Fig. 2). The experimental setup comprises an adsorption unit (Fig. 2(a)) and a displacement unit (Fig. 2(b)), with operational switching achieved through valve 3.

When valve 3 is closed, the system operates as the isothermal adsorption device. For the adsorption tests, the double-chamber equilibrium method was applied. An ISCO pump controls gas injection, and the ideal gas equation of state is used to calculate the molar quantity of gas molecules, enabling the accurate quantification of the adsorption capacity of the shale sample.

After opening valve 3, it forms a displacement experimental system. The displacement experiment was carried out on a self-built high-pressure platform. The system outlet was equipped with a high-precision flow monitor and a GC2060 gas chromatograph, enabling the real-time recording of output gas flow and the dynamic composition analysis of CH_4/CO_2.

2.3 Field test

2.3.1 Site characterization

The Nanchuan shale gas field, situated in the Pingqiao anticlinorium on the southeastern margin of the Sichuan Basin, contains proven geological reserves of nearly 0.2×10^{12} m^3, and is characterized by a low formation pressure coefficient of 1.05-1.35, satisfying the criterion for normal-pressure marine shale gas (0.9 $\leq$ pressure coefficient $<$ 1.3). The reservoir exhibits typical features of low formation energy and high adsorbed gas content. The lithology consists primarily of dark gray-black laminated carbonaceous shale and silty carbonaceous shale, with radiolarian carbon present. Siliceous shale and silty shale are the dominant rock types. The high-quality shale intervals (Table 2) have an average cumulative thickness of 40 m, a reserve abundance of 10.42×10^8 m^3/km^2, and an adsorbed gas proportion of 44%.

The integrated multi-parameter logging curves (Fig. 3) provide critical data for hydrocarbon exploration, development

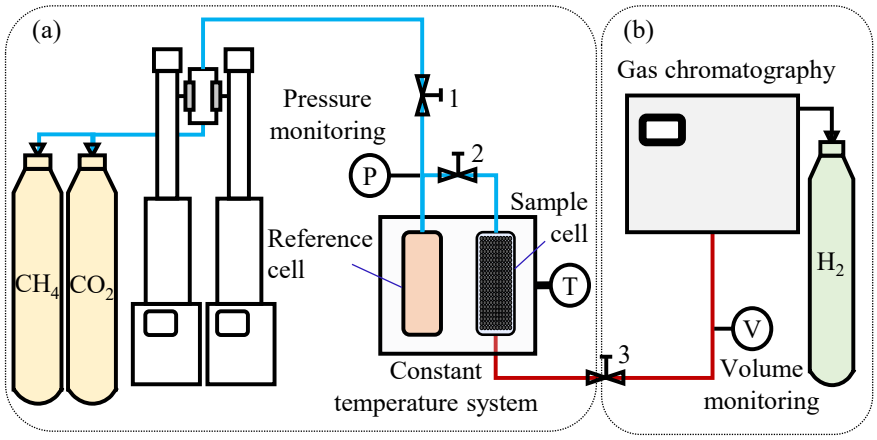

Fig. 2. Experimental system: (a) Adsorption unit and (b) displacement unit.

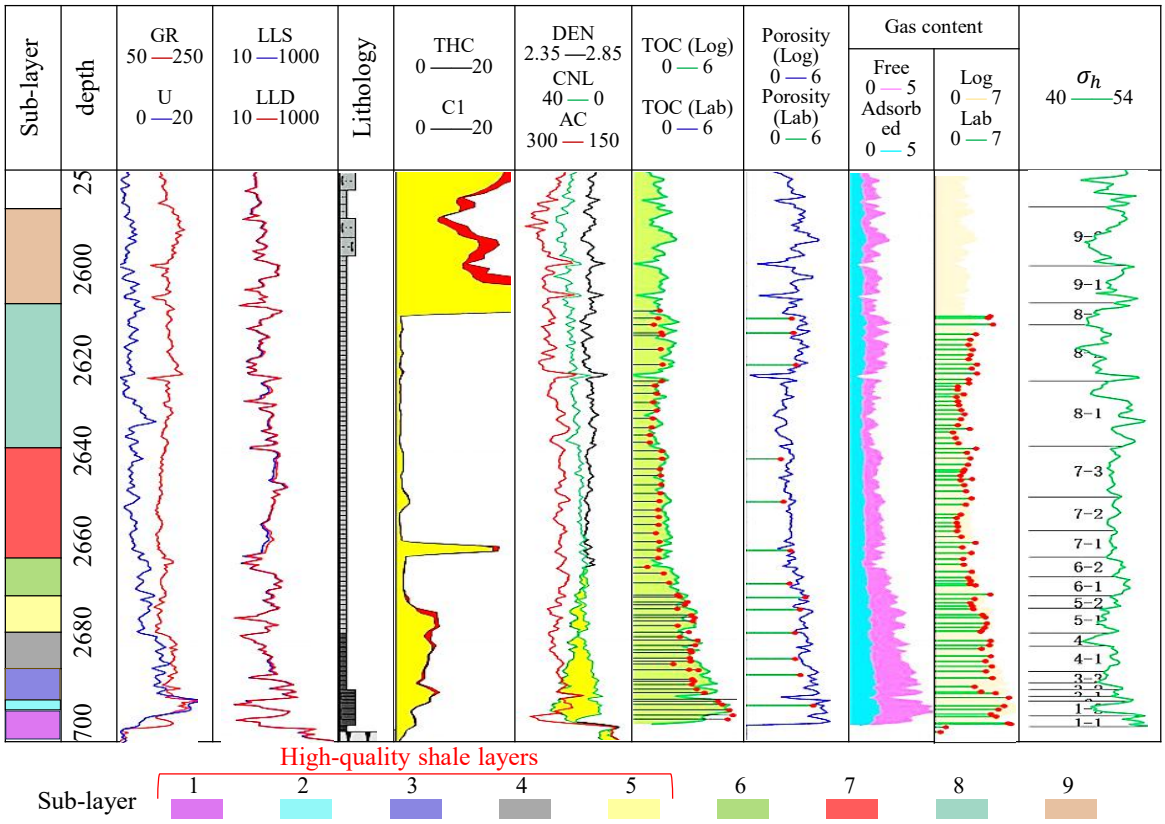

Fig. 3. Composite stratigraphic column of the Wufeng-Longmaxi formations.

and geological research. The subsurface exhibits a distinct vertical stratification composed of sub-layers 1 to 9. Lithology can be accurately identified through combined analysis of gamma ray (GR), density (DEN), and neutron (CNL) logs: High GR values indicate mudstone, while sandstone and other reservoir rocks show relatively low responses. Porosity logs directly characterize the pore development of each sub-layer, serving as a core parameter for evaluating reservoir storage capacity. Permeability is estimated empirically from porosity and lithological data. Hydrocarbon-bearing zones are evaluated by analyzing the resistivity contrast between shallow (LLS) and deep (LLD) lateral logs, complemented by total hydrocarbon content (THC) logs for quantitative evaluation. The minimum horizontal principal stress (σ_h) log offers essential mechanical parameters for understanding the *in-situ* stress state and optimizing drilling and fracturing operations.

Compared to the high-pressure Fuling shale gas reservoir, the normal-pressure Wufeng-Longmaxi Formation shale in Nanchuan exhibits distinctly different characteristics, notably a lower formation energy and a higher proportion of adsorbed gas (Shi et al., 2022). Given these specific properties, CO_2 huff and puff technology holds a significant potential to enhance

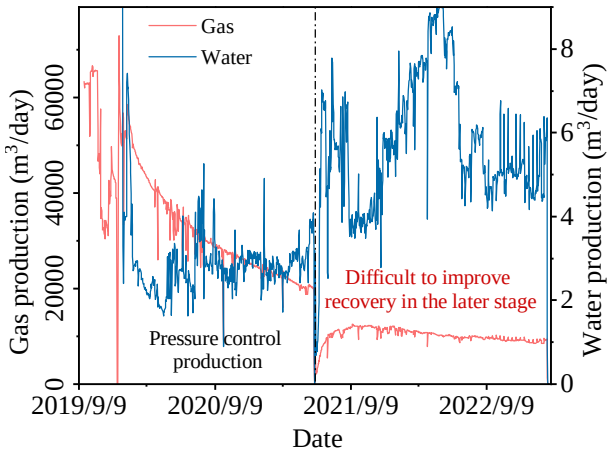

Fig. 4. Production history and stage characteristics of the test well.

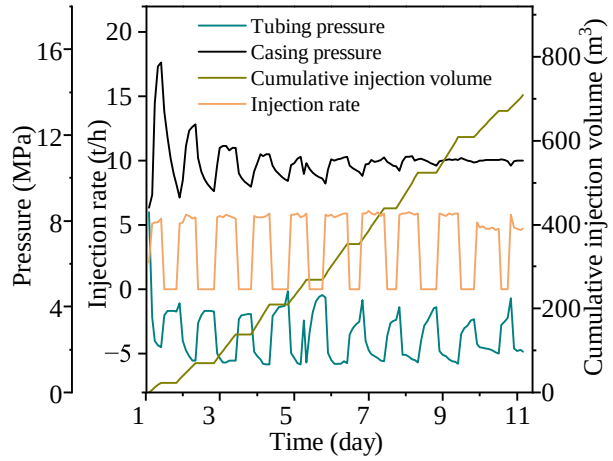

Fig. 5. Dynamic curves of wellhead pressures and CO_2 injection parameters.

the single-well production and EUR, as demonstrated in analogous reservoirs with low energy and high adsorption capacity (Liu et al., 2013, 2017, 2019). To verify this potential, gas injection huff and puff tests were conducted on selected wells in this area.

2.3.2 Production performance of test well

The test well had a vertical depth of 3,864 m and a horizontal section length of 1,659 m. It was completed with 26-stage hydraulic fracturing and produces through casing. The initial daily gas production was 60×10^3 m^3. Before CO_2 injection, the well had been in production for 1,259 days, undergoing four stages: Pressure control production, liquid unloading production increase, intermittent production, and pressurized production. The shut-in operation was performed to unload wellbore liquids, restore production, and enhance flow. In the late production stage, despite various measures to improve well drainage capacity, it became more and more difficult to maintain stable production. The well is currently in a low-pressure, production stage. The predicted EUR is 61×10^6 m^3, with a current daily gas production of 9.3×10^3 m^3 (Fig. 4) and a cumulative production of 30×10^6 m^3. The recoverable reserves at this stage account for 30%, which is an important stage for enhancing the recovery of gas wells.

2.3.3 CO_2 injection and shut-in

The cumulative amount of CO_2 injected into the test well was 708.3 t (Fig. 5). During injection, the wellhead pressure ranged from 1.3-3.5 MPa, with an average injection rate of 5.3 m^3/h. The average daily injection time was 12 hours, resulting in an average daily injection amount of 64.39 tons. The tubing was initially cleared by high injection pressure to establish stable CO_2 flow. The injection time and pressure were adjusted daily, reaching a maximum injection rate of 85.5 tons/day on the sixth day. Due to transportation constraints, daily injection remained below 100 tons. In the early stage of injection, casing pressure was significantly affected but stabilized in the later stage, indicating increased injection difficulty.

After CO_2 injection, the well was shut in for 18 days. Table 1 illustrates the temperature and pressure changes at the wellhead and the bottom hole during the shut-in event. In general, in the shut-in stage, compared with the parameters before shut-in, the most obvious change after shut-in is the bottom hole pressure, which increased by 10 MPa on average during the experiment. In contrast, other parameters remained relatively stable, showing only slight changes.

2.4 Numerical simulation

2.4.1 Governing equations

A dual-permeability model was employed to represent the shale reservoir system, conceptualized as two interacting continua: The matrix and the fracture systems. In this model, fractures provide the primary pathways for Darcy flow, while the matrix contains both free gas and adsorbed gas on the pore surfaces. The model accounts for gas desorption from the matrix, diffusion into fractures, and subsequent flow to the wellbore through the fracture network.

The mass control equation describing the fluid-rock coupled flow and mass transfer process is expressed as (Liu et al., 2016):

$$\frac{V}{\Delta t}\left(N_i^{n+1} - N_i^n\right) = \sum_k \Delta T_k \rho_k y_{ik} \Delta \phi_k + \sum_k \Delta A D_{ik} \Delta \rho_k y_{ik} + r_i + q_i \tag{5}$$

where V represents grid block volume, Δt denotes time step, N_i^n represents moles of component i at time step n, k represents fluids phase (oil (o), gas (g), or water (w)); Δ denotes difference operator, T_k denotes transmissibility, ρ_k denotes molar density, y_{ik} represents the mole fraction of component i in phase k, ϕ_k denotes porosity, D_{ik} denotes the diffusion coefficient of component i in phase k, A is an empirical correction factor for D_{ik}, r_i is source/sink term from chemical reactions, and q_i represents injection/production rate.

The Corey (1954) model is used to simulate the changes in relative permeability:

$$K_l = S^4 \tag{6}$$

$$K_g = (1-S)^2(1-S^2) \tag{7}$$

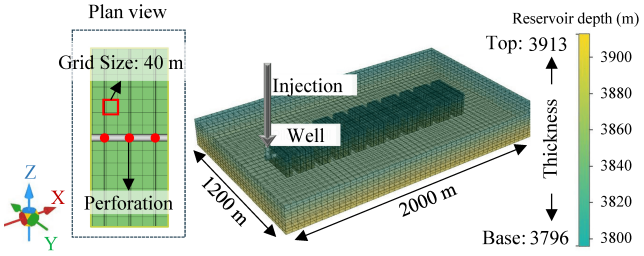

Fig. 6. Schematic of the numerical model and fracture network.

Table 3. Model parameters.

Parameters	Value	Unit
Model size	$50 \times 30 \times 10$	grid numbers
Fracture half length	125	m
Fracture height	90	m
Reservoir depth	3,796	m
$1/P_L$ of CH_4	0.00083	1/kPa
V_L of CH_4	0.08	mole/kg
$1/P_L$ of CO_2	0.001	1/kPa
V_L of CO_2	0.18	mole/kg
3-dimension permeability	0.0001, 0.0001, 0.00001	md

$$S = \frac{S_l - S_{lr}}{1 - S_{lr} - S_{gr}} \tag{8}$$

where S denotes normalized saturation, K_l and K_g respectively denote liquid and gas relative permeability, S_l represents liquid saturation, S_{lr} denotes irreducible liquid saturation, and S_{gr} is residual gas saturation.

The gas adsorption behavior follows the extended Langmuir isotherm mode (Zhan et al., 2021):

$$C_i = \frac{C_{im} B_i y_{ig} P}{1 + P \sum_i B_i y_{ig}} \tag{9}$$

where C_i represents the adsorbed amount of component i per rock mass, C_{im} represents the maximum adsorption capacity of component i, B_i is a Langmuir constant for component i, y_{ig} is mole fraction of component i in gas phase, and P is pressure.

Residual gas saturation is predicted using the Land (1968) model:

$$S_{gr} = S_{gc} + \frac{S_{gm} - S_{gc}}{1 + C(S_{gm} - S_{gc})} \tag{10}$$

where S_{gr} represents residual gas saturation, S_{gc} represents critical gas saturation; S_{gm} represents maximum gas saturation, and C is Land parameter calculated from S_{gc}.

2.4.2 Model setup

To evaluate the displacement efficiency and storage potential in the Nanchuan shale gas reservoir, a three-dimensional, dual-permeability numerical model was constructed using the CMG-GEM compositional simulator (Zhang et al., 2021). This model simplifies the reservoir into two interacting continua: A matrix system governing gas storage and transport in nano- to micropores, and a fracture system accounting for rapid flow through natural and hydraulic fractures. Gas adsorption and desorption for CH_4 and CO_2 are represented by the Langmuir and extended Langmuir isotherm models, respectively, while the effects of aqueous phase and geomechanical responses are neglected to focus on the fundamental mechanisms of gas-phase transport and competitive adsorption.

The reservoir was initialized with pure CH_4 at 40 MPa and 383K, consistent with observed pressure and temperature gradients. Closed boundary conditions were applied to represent a volumetrically bounded reservoir. Local grid refinement was employed near the wellbore and fractures, with the grid sizes progressively reduced from 50 m in the matrix to 0.5 m near the well (Fig. 6). The key model parameters are summarized in Table 3.

2.4.3 Simulation workflow

To ensure the predictive reliability of the model, it was first calibrated via history matching using production data from the field test. The validated model then simulated the CO_2 huff and puff process, with CH_4/CO_2 displacement and storage dynamics monitored through the component tracking module of CMG. Eight huff and puff scenarios were set up to investigate the effects of CO_2 injection amount, shut-in time, and injection timing on shale gas recovery (Table 4). Group1 served as the control group, Group 2 and Group 3 corresponded to different CO_2 injection amounts, and the main control parameter was the STG of the injection well. Group 4 and group 5 were set up to evaluate different shut-in times. Groups 6-8 were created to assess different CO_2 injection timings.

3. Results

3.1 Isothermal adsorption

CH_4 isothermal adsorption data for the crushed core samples at 90 °C were fitted using the Langmuir equation. Samples A1-A3 and B1-B10 were collected from two distinct wells. The high coefficients of determination ($R^2 > 0.97$) demonstrated excellent fitting performance, confirming the applicability of the Langmuir model for characterizing shale adsorption behavior (Table 5).

Subsequently, three sets of experiments were designed to investigate CH_4 and CO_2 adsorption on shale at 30, 60 and 90 °C. As illustrated in the isothermal adsorption curves (Fig. 7), temperature exhibits an inhibitory effect on adsorption, while pressure promotes adsorption within a certain range. Notably, CO_2 has a maximum adsorption capacity two times higher than that of CH_4. For instance, at 60 °C and 6 MPa, the CO_2 adsorption capacity reaches 0.18 mol/kg, compared to 0.09 mol/kg for CH_4, highlighting the stronger adsorption affinity of CO_2 for the shale matrix.

The CO_2 adsorption curve at 30 °C exhibits a distinct trend compared to other temperatures. Repeated experiments obtain-

Table 4. Parameter settings for the simulation scenarios.

Variable description	Group	Injection amount (tons)	Shut-in time (days)	Injection timing (date)
Control group	1	2,500	20	2023-03-02
Injection amount	2	1,600	20	2023-03-02
	3	900	20	2023-03-02
Shut-in time	4	2,500	60	2023-03-02
	5	2,500	5	2023-03-02
Injection timing	6	2,500	20	2022-03-02
	7	2,500	20	2021-03-02
	8	2,500	20	2020-03-02

Table 5. Langmuir parameters for CH_4 adsorption isotherms at 90 °C.

No.	Well depth (m)	V_L (cm^3/g)	P_L (MPa)	R^2
A1	3,391.00	1.88	1.71	0.98
A2	3,395.27	1.41	1.55	0.98
A3	3,397.35	1.43	1.33	0.98
B1	3,695.41	1.21	1.62	0.97
B2	3,700.36	0.70	1.16	0.99
B3	3,705.39	0.74	1.40	0.98
B4	3,715.46	0.67	0.69	0.98
B5	3,727.50	0.63	1.04	0.98
B6	3,737.50	1.41	1.20	0.99
B7	3,740.15	1.14	1.53	0.98
B8	3,742.42	1.46	0.96	0.99
B9	3,746.06	3.26	1.09	0.99
B10	3,749.84	1.37	0.93	0.98

ed reproducible trend curves, while the 40 °C isothermal adsorption curve showed no significant increase. This suggests that the inhibition effect of temperature on adsorption is less pronounced near the CO_2 phase transition critical point, leading to different adsorption characteristics. For the 30 °C adsorption curve, the Brunauer-Emmett-Teller model provides a better fit to the experimental data than the Langmuir equation (Marlow, 2014). The slight deviations in the repeated experiments are attributed to challenges in maintaining a constant temperature near ambient conditions during manual pressurization.

3.2 CO_2 displacement

To evaluate the effects of CO_2 injection pressure (3-6 MPa) and injection rate (10-40 mL/min) on CH_4 displacement efficiency, systematic displacement experiments were conducted using CH_4 pre-adsorbed shale samples.

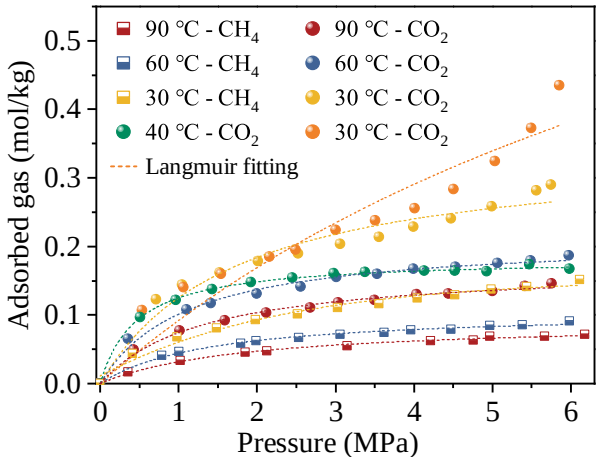

Fig. 7. Isothermal adsorption curves.

As depicted in Fig. 8, the experimental data reveal that the breakthrough time of CO_2 is notably influenced by the injection pressure. Higher injection pressures are associated with a faster penetration rate of CO_2; however, this also results in a longer duration required for CO_2 to achieve 90% displacement efficiency of CH_4. Additionally, when the injection rate is held constant at 10 mL/min, pressure fluctuations within the range of ±0.3 MPa lead to a fluctuation coefficient of 8.7% in the produced gas composition. This indicates that the influence of the injection rate parameter on displacement efficiency is significantly less pronounced compared to that of the pressure parameter.

3.3 Pilot test performance

Two rounds of CO_2 huff and puff operations were implemented in Well JY201-3HF. The first round, involving the injection of 700 tons of CO_2, natural gas production increased by 134.9×10^4 m^3 (average of 1.2×10^4 m^3/day) and the CO_2 backflow rate reached 94%. For the second round, with 1300 tons of CO_2 injected, the average daily yield increased by 1.02×10^4 m^3, and the flowback rate decreased to 19%.

The comparative analysis of the first round of huff and puff shows that CO_2 huff and puff significantly improved gas well production, which was better than the traditional production mode of direct shut-in recovery pressure. After CO_2 injection, the average daily gas production increased from 0.95×10^4 to 1.75×10^4 m^3, as presented in Fig. 9. Material balance analysis predicted a single-well EUR rise from 0.75×10^8 to 0.9×10^8 m^3, the reserves of single well at 5.186×10^8 m^3, and the increase in expected recovery from 14.5% to 17.4%, an increase of 2.9%, showing good production potential and application prospects.

The evolution characteristics of gas components (Fig. 10) show that the content of CO_2 decreased from 46.67% to 6.03%, and the content of CH_4 increased from 52.89% to 92.97%, which confirms the effective displacement of CO_2. The production calculation based on component analysis shows that in the three months after the well was opened, the cumulative gas production was 190.73×10^4 m^3, of which

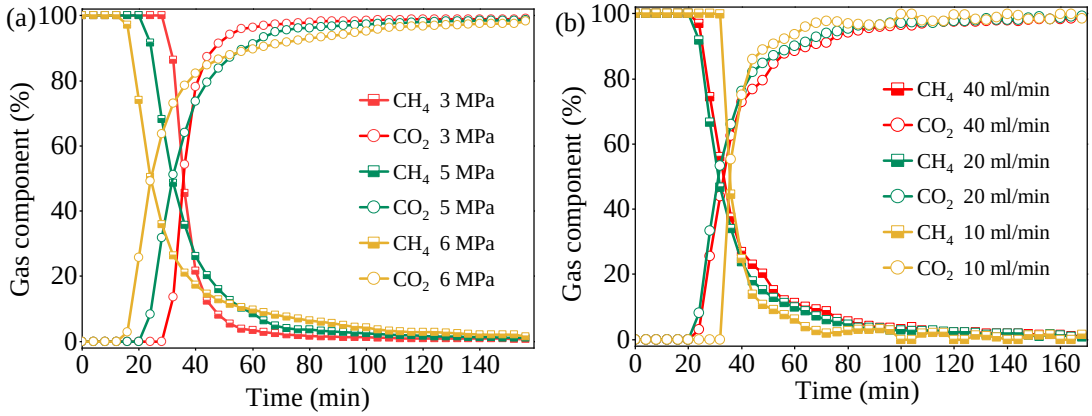

Fig. 8. Compositional changes during CO_2 displacement under varying (a) injection pressure and (b) injection rate.

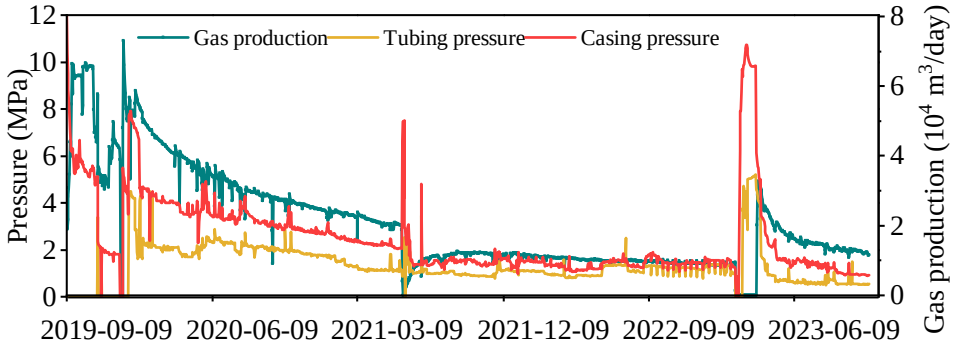

Fig. 9. CO_2 huff and puff production characteristics in the test well.

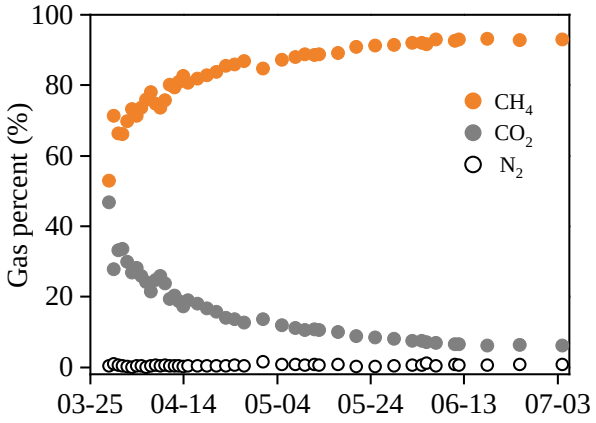

Fig. 10. Gas percent during CO_2 huff and puff production.

CH_4 accounted for 163.14×10^4 m^3, CO_2 was 26.20×10^4 m^3, and the carbon storage rate was 26.1%. This effective sequestration aligns with the mechanisms observed in CO_2 flooding in ultra-low permeability sandstones, where a significant portion of injected CO_2 is immobilized through various trapping mechanisms (Liu et al., 2025c). The CO_2 huff and puff test results for this pilot well demonstrates that CO_2 injection effectively enhances the reservoir energy through pore pressure increase, promoting CH_4 desorption and production.

3.4 Model verification

Through a global sensitivity analysis performed with CMG-CMOST, the influence of key parameters on production forecasting was quantified. The results indicate that fracture conductivity and Langmuir volume are the dominant factors, contributing 42% and 28% to production prediction, respectively. For every 1 percentage point increase in permeability and porosity, the recovery increases by 0.8%-1.2%.

The model calibrated by automatic parameter inversion can accurately reproduce the actual production dynamics, with the history matching results shown in Fig. 11. The goodness of fit for critical reservoir parameters including permeability, porosity, water saturation, and fracture properties (conductivity, half length) are all above 0.9. In particular, the model uses the experimentally measured Langmuir parameters (CO_2: 0.18 mol/kg, CH_4: 0.08 mol/kg) and diffusion coefficient (CO_2: 8.5×10^{10} cm^2/s, CH_4: 1.2×10^{10} cm^2/s) to accurately simulate competitive adsorption behavior in the shale reservoir.

Taking the validated model as a basis, various injection schemes were designed to study the influence of gas injection amount, shut-in time and injection timing on well production. The prediction error was controlled within 8%. By optimizing the CO_2 injection parameters, this analysis provides a theoretical basis for the further development of shale gas reservoirs. It should be noted that the purpose of planned shut-in during sand cleaning operation is to stabilize downhole pressure, facilitate effective sand discharge, and reduce equipment cor–

Table 6. Comparison of shale adsorption characteristics among different blocks.

Sampling block	Formation pressure factor	Mineral constituent (%)			45 °C, 3 MPa Adsorption quantity (mol/kg)	
		Quartz	Clay minerals	Others	CH_4	CO_2
Yanchang	0.80-0.90	42.14	47.65	10.21	0.035	0.085
Changning	1.30-2.00	53.11	32.73	14.16	0.056	0.127
Nanchuan	1.05-1.35	54.40	22.74	22.86	0.122	0.211

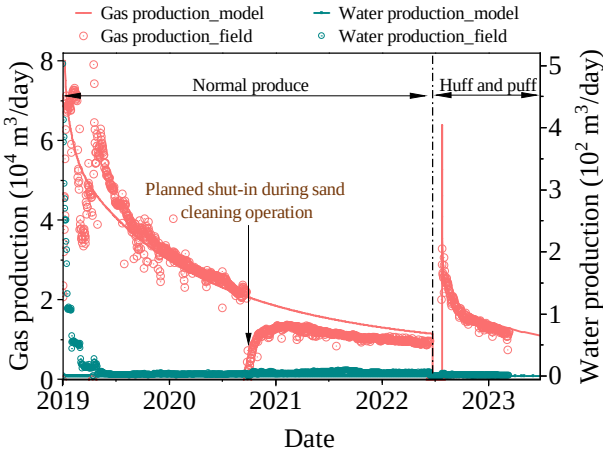

Fig. 11. History matching results of gas well production performance.

rosion by reducing fluid flow rate, so as to ensure operational safety and maintain wellbore integrity.

4. Discussion

4.1 CO_2 displacement potential of Nanchuan shale

The technical feasibility of enhanced gas recovery by injecting CO_2 into normal-pressure marine shale reservoirs is supported by a multi-scale mass transfer mechanism. From the molecular scale, CO_2 has a smaller kinetic diameter and molar mass than CH_4, resulting in a Knudsen diffusion coefficient that is 1-2 orders of magnitude higher, demonstrating superior mass transfer ability in nanoscale pores. Concurrently, the stronger surface affinity of CO_2 promotes surface diffusion and effectively replaces the adsorbed CH_4 through competitive adsorption. The experimental data show that the adsorption ability of CO_2 is 30%-50% stronger than that of CH_4 at 45 °C/3MPa. This is a dual advantage that is particularly significant in reservoirs with strong pore connectivity. Darcy flow in macropores (> 50 nm) and diffusion mass transfer in micropores (< 2 nm) collectively enhance gas recovery.

The CH_4/CO_2 mass transfer in shale is controlled by temperature-pressure-pore structure coupling. Increasing temperature enhances molecular thermal motion, increasing the Knudsen diffusion coefficient by 20%-30% and reducing gas viscosity by 5%-8%, thus improving the Darcy seepage conditions. The pressure system shows a dual effect: Before the critical adsorption pressure is reached, the pressure increase promotes adsorption and enhances surface diffusion; meanwhile, as the driving force of seepage, the increase of pressure gradient can also increase the seepage velocity by 30%-50%. Furthermore, the miscibility and pore-scale confinement effects can significantly alter the fluid phase behavior and transport efficiency, adding another layer of complexity to the multi-scale recovery mechanism (Chen et al., 2022).

By comparing the reservoir characteristics and adsorption properties of the three typical blocks (Table 6), it is found that the mass transfer advantage of Nanchuan normal pressure shale has a clear geological origin. The high brittle mineral content in this block forms a developed pore network. The micro-nanopores provide an ideal channel for Knudsen diffusion and the permeability is relatively improved. Under the same conditions, the level of CO_2 adsorption at 0.211 mol/kg is significantly higher than that of the Changning (0.127 mol/kg) and Yanchang blocks (0.085 mol/kg) (Du et al., 2019). This difference shows a significant positive correlation with the pore structure parameters including adsorption surface area and pore size distribution. Notably, the low clay mineral content in the Nanchuan shale effectively reduces the binding effect on gas molecules and increases surface diffusion ability. These characteristics provide an important geological basis and engineering targets for optimizing CO_2-ESGR technology in normal-pressure shale gas reservoirs.

4.2 Optimization of CO_2 injection amount

The simulation results of CO_2 huff and puff show that increased CO_2 injection boosts single-well cumulative gas production, as presented in Fig. 12(a). This is attributed to two mechanisms: Enhanced competitive adsorption (raising the adsorption replacement efficiency by 38%-48%) and improved reservoir pressure maintenance (reducing the pressure attenuation by 30%-40%), which are shown in Fig. 13(a). Similar to other gas reservoirs, a larger CO_2 injection amount generally benefits adsorption replacement and storage. However, when injection exceeds 0.8 PV (pore volume), gas channeling occurs, advancing CO_2 breakthrough and decreasing CH_4 recovery by 5%-8%, suggesting that the injection interval has an optimal value.

Based on the current engineering practice and the numerical simulation results of normal-pressure marine shale, the optimal injection range of CO_2 was determined to be 0.2-0.5 PV. This injection range ensures balanced CO_2 diffusion

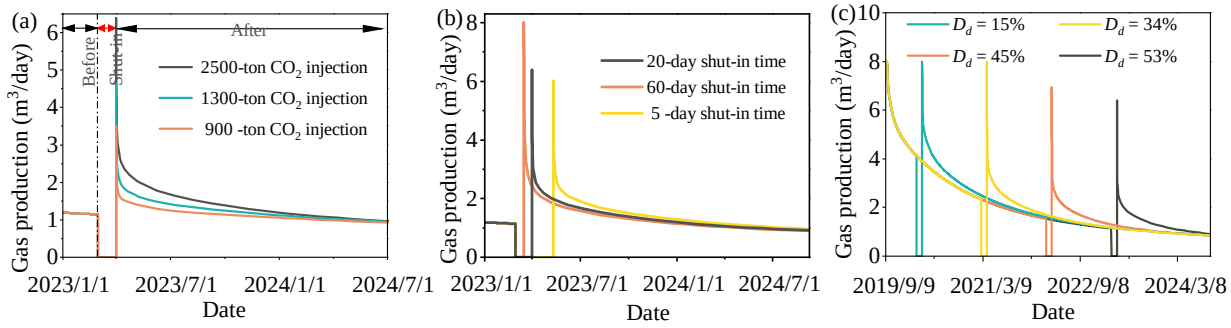

Fig. 12. Sensitivity analysis of huff and puff: (a) Effect of injection amount, (b) shut-in time and (c) injection timing on gas production.

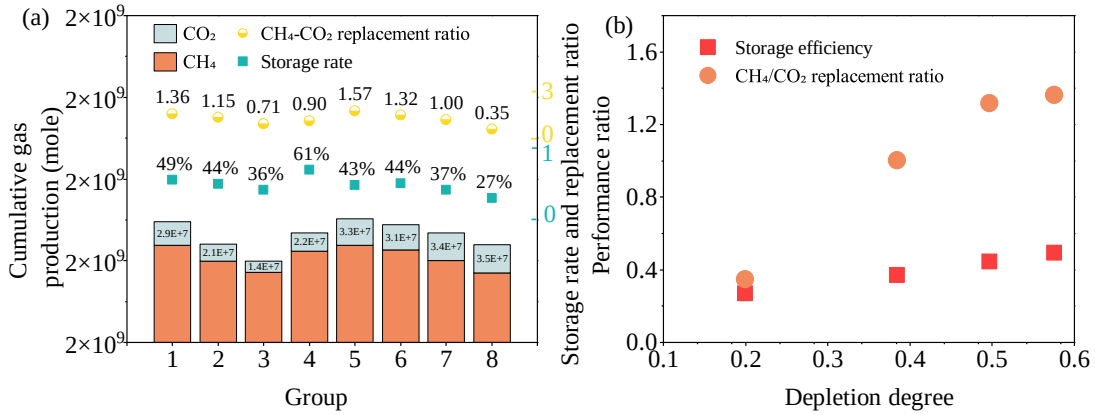

Fig. 13. Simulation analysis: (a) Cumulative gas production and CO_2 storage-displacement effects and (b) depletion degree effect.

within the matrix-fracture system while maximizing marginal benefits when the single-cycle production increase reaches 8%-12%. Moreover, it aligns well with the operational capacity range of 2-5 m^3/min of conventional injection equipment.

Herein, an innovative stepwise low-dose multi-cycle injection strategy is proposed. In the initial cycle, a relatively low injection amount (within the 0.2-0.5 PV range) is applied to establish a baseline CO_2 saturation in the matrix. Subsequently, the injection amount is incrementally increased by 15% per cycle, with dynamic adjustments based on compositional changes in produced gas from previous cycles. This approach enhances ultimate recovery while minimizing CO_2 leakage, thereby optimizing overall development efficiency.

4.3 Shut-in time effect

As shown in Fig. 12(b) the simulation results reveal the influence mechanism of shut-in time on the interaction of CO_2-shale. Shut-in time is a key parameter to regulate the interaction between CO_2 and shale, and its duration directly affects the gas diffusion depth and displacement efficiency (Tai and Gates 2024). Short-term shut-in (< 7 days) is found to cause CO_2 to fail to fully diffuse to nanoscale pores, resulting in a 30%-40% reduction in the adsorption replacement efficiency. Although long-term shut-in (> 30 days) can increase the CH_4 desorption rate to 1.8 times the reference value, it will lead to prolonged production cycle and diminishing marginal benefits where the increase is only 2%-3% for every 10 days.

A correlation exists between reservoir pressure dynamics and gas production characteristics, with the shut-in process having a decisive influence on reservoir pressure recovery and gas migration mode (Keles et al., 2020). In the early development stage, free gas is mainly produced (accounting for more than 70%). As formation pressure declines, the proportion of adsorbed gas desorption gradually increases, reaching 60%-80% in the late development stage. Numerical simulations indicate that the high adsorbed gas content ($> 45\%$) of Nanchuan shale gas wells determines its long-term production potential, and a moderate shut-in time (5-60 days) can effectively stimulate the desorption of adsorbed gas in nanopores.

Extended shut-in (60 days) expands the gas sweep range. After 60 days of shut-in, the proportion of CO_2 diffusion and storage in the normal pressure shale reservoir reaches 61%, which is significantly better than that of the short-term shut-in scheme ($< 50\%$). This feature helps maintain stable productivity in the late stage of depletion wells. However, the gas production effect of 60-day shut-in is significantly reduced, and the replacement efficiency is also 43% lower than that of short-term shut-in (5 days).

On the basis of the reservoir characteristics and development economics, a differentiated shut-in strategy is proposed. For production wells with the goal of rapid production boost,

short-term shut-in (5-7 days) can be implemented. Although the gas storage rate is reduced in this case, the single-cycle production and replacement efficiency can still be improved. For reservoirs that focus on improving ultimate recovery, it is recommended to use medium- and long-term shut-in (15-60 days) to increase cumulative production by fully stimulating the potential of adsorbed gas. It is particularly noteworthy that although the short-term shut-in scheme is not conducive to CO_2 sequestration (12%-30% reduction), the multi-cycle huff and puff production mode is better suited to the development characteristics of normal-pressure shale gas wells, achieving an optimal balance between gas recovery and economic efficiency.

4.4 Optimal CO_2 injection timing

The degree of reservoir depletion D_d was quantitatively characterized on the basis of the proportion of cumulative gas production (Wang et al., 2025a):

$$D_d = \frac{Q_c}{Q_c + G_r} \times 100\% \tag{11}$$

where Q_c denotes cumulative gas production, and G_r denotes the remaining reserves. The correlation analysis between the degree of depletion and the effect of CO_2 indicates that the gas injection timing has a significant regulatory effect on the CO_2 huff and puff performance (Fig. 12(c)) The degree of depletion D_d is significantly positively correlated with the CO_2 sequestration rate, but when $D_d > 60\%$, the growth rate slows down (Fig. 13(b)). The relationship between R and CH_4 replacement ratio increases first and then decreases, reaching a maximum of 2.1 at $D_d = 45\%$, and then decreases by 15%-20% due to the deterioration of matrix permeability.

The nonlinear response results from the coupling of three mechanisms. At low pressures, CO_2 adsorption site saturation drops by 20%-25% when a certain condition exceeds 50%. Stress sensitivity closes the seepage channels, causing 30%-40% permeability loss. Micro-nano pore competitive adsorption kinetics change, reducing surface diffusion contribution by 15%-18%. These findings help to optimize the CO_2 huff and puff strategy for normal-pressure shale gas reservoirs.

The choice of CO_2 injection timing is essentially a dynamic balance between reservoir energy maintenance and gas replacement. Early gas injection ($D_d = 60\%$) will reduce the matrix permeability due to stress sensitivity, making desorption more and more difficult. In the medium depletion stage ($D_d = 45\%$-55%), the CO_2 sequestration rate and the CH_4/CO_2 replacement ratio can reach the peak synchronously, and the mass transfer efficiency of the matrix-fracture system is the best.

Adsorbed gas is crucial for CO_2 sequestration and CH_4 production, contributing 2-3 times more than free gas. Normal-pressure shale in the Nanchuan block has over 40% adsorbed gas and a well-developed pore network (70% of pores < 5 nm), ideal for CO_2-ESGR. The simulation shows that an injection parameter combination of 0.3-0.5 PV injection amount, 45%-55% pressure attenuation during medium-term injection, and 15-60 days of shut-in maximizes gas recovery and CO_2 sequestration; this combination optimizes the interactions between CO_2 injection and shale reservoir properties, guiding local CO_2-ESGR field applications.

5. Conclusions

With the aim to evaluate the feasibility and potential of CO_2 huff and puff of normal-pressure marine shale gas, this study presents a refined numerical model by integrating data from laboratory experiments and a field injection test. The key findings are as follows:

1) The Nanchuan shale exhibits a strong preferential adsorption for CO_2 over CH_4, with a CO_2 adsorption capacity of 0.211 mol/kg at 45 °C and 3 MPa, approximately twice that of CH_4 and significantly higher than its counterparts in the Changning and Yanchang blocks. This fundamental property is a cornerstone for both enhanced recovery and effective CO_2 sequestration.
2) China's first field pilot test in a normal-pressure shale gas reservoir demonstrated direct success. The EUR of a single well was boosted by 2.9%, increasing daily gas production from 9.5×10^3 to 17.5×10^3 m^3. The analysis confirmed a carbon storage ratio of 26.1% during the production phase, validating the dual objectives of the technology.
3) Our sensitivity analysis based on the history-matched model identified a precise operational envelope for maximum efficiency. The optimal strategy involves injecting 0.3-0.5 pore volumes of CO_2 when reservoir pressure depletion reaches 45%-55%, followed by a controlled shut-in period of 15-60 days. Adhering to this window maximizes CH_4 displacement while ensuring significant CO_2 storage.

Acknowledgements

This research was supported by the Science Fund for Distinguished Young Scholars of Chongqing Municipality (No. cstc2021jcyj-jqX0007), the Chongqing Science and Technology Foundation (Nos. CSTB2023TIAD-KPX0082 and CSTB2024TIAD-KPX0086) and the Science and Technology Department of China Petrochemical Corporation (Nos. P24115 and P25127).

Conflict of interest

The authors declare no competing interest.

References

Afari, S., Ling, K., Maxey, D., et al. Experimental investigation of gaseous solvent huff-n-puff in the Middle Bakken Formation. Petroleum Science, 2023, 20: 3488-3497.

Chang, X., Lin, S., Yang, C., et al. A critical review of $ScCO_2$-enhanced gas recovery and geologic storage in shale reservoirs. Gas Science and Engineering, 2024, 125: 205327.

Chen, H., Liu, X., Zhang, C., et al. Effects of miscible degree and pore scale on seepage characteristics of unconventional reservoirs fluids due to supercritical CO_2 injection. Energy, 2022, 239: 122287.

Corey, A. T. The interrelation between gas and oil relative permeabilities. Producers Monthly, 1954, 19(1): 38-41.

Duan, S., Gu, M., Du, X., et al. Adsorption equilibrium of CO_2 and CH_4 and their mixture on Sichuan Basin shale. Energy & Fuels, 2016, 30(3): 2248-2256.

Du, X., Gu, M., Duan, S., et al. The influences of CO_2 injection pressure on CO_2 dispersion and the mechanism of CO_2-CH_4 displacement in shale. Journal of Energy Resources Technology, 2017, 140(1): 012907.

Du, X., Gu, M., Hou, Z., et al. Experimental study on the kinetics of adsorption of CO_2 and CH_4 in gas-bearing shale reservoirs. Energy & Fuels, 2019, 33(12): 12587-12600.

Godec, M., Koperna, G., Petrusak, R., et al. Potential for enhanced gas recovery and CO_2 storage in the Marcellus Shale in the Eastern United States. International Journal of Coal Geology, 2013, 118: 95-104.

Godec, M., Koperna, G., Petrusak, R., et al. Enhanced gas recovery and CO_2 storage in gas shales: A summary review of its status and potential. Energy Procedia, 2014, 63: 5849-5857.

Gu, M., Xian, X., Duan, S., et al. Influences of the composition and pore structure of a shale on its selective adsorption of CO_2 over CH_4. Journal of Natural Gas Science and Engineering, 2017, 46: 296-306.

Hamza, A., Hussein, I., Al-Marri, M., et al. CO_2 enhanced gas recovery and sequestration in depleted gas reservoirs: A review. Journal of Petroleum Science and Engineering, 2021, 196: 107685.

Hu, X., Deng, H., Lu, C., et al. Characterization of CO_2/CH_4 competitive adsorption in various clay minerals in relation to shale gas recovery from molecular simulation. Energy & Fuels, 2019, 33(9): 8202-8214.

Iddphonce, R., Wang, J. Investigation of CO_2 and CH_4 competitive adsorption during enhanced shale gas production. Journal of Petroleum Science and Engineering, 2021, 205: 108802.

Jia, B., Chen, Z., Xian, C. Investigations of CO_2 storage capacity and flow behavior in shale formation. Journal of Petroleum Science and Engineering, 2022, 208: 109659.

Keles, C., Tang, X., Schlosser, C., et al. Sensitivity and history match analysis of a carbon dioxide 'huff-and-puff' injection test in a horizontal shale gas well in Tennessee. Journal of Natural Gas Science and Engineering, 2020, 77: 103226.

Land, C. S. Calculation of imbibition relative permeability for two- and three-phase flow from rock properties. Society of Petroleum Engineers Journal, 1968, 8(2): 149-156.

Liao, Q., Zhou, J., Xian, X., et al. Competition adsorption of CO_2/CH_4 in shale: Implications for CO_2 sequestration with enhanced gas recovery. Fuel, 2023, 339: 127400.

Liu, D., Li, Y., Agarwal, R. K. Numerical simulation of long-term storage of CO_2 in Yanchang shale reservoir of the Ordos Basin in China. Chemical Geology, 2016, 440: 288-305.

Liu, F., Ellett, K., Xiao, Y., et al. Assessing the feasibility of CO_2 storage in the New Albany Shale (Devonian-Mississippian) with potential enhanced gas recovery using reservoir simulation. International Journal of Greenhouse Gas Control, 2013, 17: 111-126.

Liu, J., Xie, M., Liu, D., et al. Research on mechanism and effect of enhancing gas recovery by CO_2 huff-n-puff in shale gas reservoir. ACS Omega, 2024, 9: 33111-33118.

Liu, J., Xiao, D., Li, J., et al. Enhanced oil recovery via CO_2 flooding in tight reservoirs: A pore-scale analysis. Advances in Geo-Energy Research, 2025a, 17(2): 162-175.

Liu, J., Xie, L., Elsworth, D., et al. CO_2/CH_4 competitive adsorption in shale: Implications for enhancement in gas production and reduction in carbon emissions. Environmental Science & Technology, 2019, 53(15): 9328-9336.

Liu, J., Yao, Y., Liu, D., et al. Experimental evaluation of CO_2 enhanced recovery of adsorbed-gas from shale. International Journal of Coal Geology, 2017, 179: 211-218.

Liu, X., Chen, H., Cheng, W., et al. Occurrence states and transport behavior of crude oil in different permeability oil reservoirs during depletion development. Geoenergy Science and Engineering, 2025b, 252: 213944.

Liu, X., Chen, H., Li, Y., et al. Oil production characteristics and CO_2 storage mechanisms of CO_2 flooding in ultra-low permeability sandstone oil reservoirs. Petroleum Exploration and Development, 2025c, 52: 196-207.

Li, W., Cao, J., Liang, Y., et al. Evaluation of CO_2 storage and enhanced gas recovery potential in gas shale using kerogen nanopore systems with mesopores and micropores. Chemical Engineering Journal, 2024, 486: 150225.

Louk, K., Ripepi, N., Luxbacher, K., et al. Monitoring CO_2 storage and enhanced gas recovery in unconventional shale reservoirs: Results from the Morgan County, Tennessee injection test. Journal of Natural Gas Science and Engineering, 2017, 45: 11-25.

Lu, T., Zeng, K., Jiang, P., et al. Competitive adsorption in CO_2 enhancing shale gas: Low-field NMR measurement combined with molecular simulation for selectivity and displacement efficiency model. Chemical Engineering Journal, 2022, 440: 135865.

Marlow, J. Characterizing geological and geochemical properties of selected gas shales and their thermal maturation in the Black Warrior Basin, Alabama. Auburn, Auburn University, 2014.

Omari, A., Wang, C., Li, Y., et al. The progress of enhanced gas recovery (EGR) in shale gas reservoirs: A review of theory, experiments, and simulations. Journal of Petroleum Science and Engineering, 2022, 213: 110461.

Shi, W., Zhang, C., Jiang, S., et al. Study on pressure-boosting stimulation technology in shale gas horizontal wells in the Fuling Shale Gas Field. Energy, 2022, 254: 124364.

Song, Y., Song, Z., Chen, Z., et al. Simulation of CO_2 enhanced oil recovery and storage in shale oil reservoirs: Unveiling the impacts of nano-confinement and oil composition. Advances in Geo-Energy Research, 2024, 13(2):

106-118.

Tai, N., Gates, I. Cyclic CO_2 storage and geothermal energy extraction using a huff and puff technique in the Basal Cambrian Sandstone Unit, Canada. Geothermics, 2024, 118: 102925.

Tang, C., Zhou, W., Chen, Z., et al. Numerical simulation of CO_2 sequestration in shale gas reservoirs at reservoir scale coupled with enhanced gas recovery. Energy, 2023, 277: 127657.

Wang, H., Li, G., Shen, Z. A feasibility analysis on shale gas exploitation with supercritical carbon dioxide. Energy Sources, Part A: Recovery, Utilization, and Environmental Effects, 2012, 34(15): 1426-1435.

Wang, H., Zhou, J., Xian, X., et al. Shale gas production and CO_2 storage of CO_2-ESGR based on the stress-strain-sorption behavior of shale. Energy & Fuels, 2025a, 39(11): 5406-5418.

Wang, Y., Cao, R., Jia, Z., et al. A multi-mechanism numerical simulation model for CO_2-EOR and storage in fractured shale oil reservoirs. Petroleum Science, 2024, 21: 1814-1828.

Wang, Y., Wang, J., Liu, H., et al. Effects of gas components on acid-rock reaction during CO_2-contained industrial waste gas (CO_2-contained IWG) injection into deep shale reservoir on geologic time scale. Petroleum Science, 2025b, 22: 2604-2618.

Xie, W., Wang, H., Vandeginste, V., et al. Thermodynamic and kinetic affinity of CO_2 relative to CH_4 and their pressure, temperature and pore structure sensitivity in the competitive adsorption system in shale gas reservoirs. Energy, 2023, 277: 127591.

Yang, K., Zhou, J., Xian, X., et al. Adsorption characteristics and thermodynamic analysis of CH_4 and CO_2 on continental and marine shale. Transport in Porous Media, 2021, 140(3): 763-788.

Yang, N., Liu, S., Yang, X. Molecular simulation of preferential adsorption of CO_2 over CH_4 in Na-montmorillonite clay material. Applied Surface Science, 2015, 356: 1262-1271.

Yang, Q., Huang, L., Chen, Q., et al. Molecular insights into CO_2 sequestration and enhanced gas recovery in water-bearing shale nanocomposites. Separation and Purification Technology, 2025, 355: 129618.

Yu, X., Dong, H., Li, Y., et al. Microscopic insights into CO_2-shale oil miscibility via interaction energy coupled with pore confinement: Implications for CO_2-enhanced oil recovery. Advances in Geo-Energy Research, 2025, 17(2): 107-120.

Zhang, H., Diao, R., Chan, H., et al. Deformation of shale and coal organic carbon slit micropores induced by CO_2-enhanced gas recovery: A Monte Carlo simulation study. Energy & Fuels, 2020, 34(2): 1564-1580.

Zhang, L., Zhang, T., Zhao, Y., et al. A review of interaction mechanisms and microscopic simulation methods for CO_2-water-rock system. Petroleum Exploration and Development, 2024, 51(1): 223-238.

Zhang, R., Wu, J., Zhao, Y., et al. Numerical simulation of the feasibility of supercritical CO_2 storage and enhanced shale gas recovery considering complex fracture networks. Journal of Petroleum Science and Engineering, 2021, 204: 108671.

Zhan, J., Niu, Z., Li, M., et al. Numerical simulation and modeling on CO_2 sequestration coupled with enhanced gas recovery in shale gas reservoirs. Geofluids, 2021, 2021: 9975296.

Zhao, X., Chen, Z., Wang, B., et al. A multi-medium and multi-mechanism model for CO_2 injection and storage in fractured shale gas reservoirs. Fuel, 2023, 345: 128167.

Zhao, Y., Luo, M., Zhang, T., et al. Competitive adsorption of CH_4/CO_2 in shale nanopores during static and displacement process. Natural Gas Industry B, 2024, 11(3): 239-251.

Zhou, G., Duan, X., Chang, J., et al. Investigation of CH_4/CO_2 competitive adsorption-desorption mechanisms for enhanced shale gas production and carbon sequestration using nuclear magnetic resonance. Energy, 2023, 278: 127964.

Zou, C., Zhao, Q., Dong, D., et al. Geological characteristics and resource potential of shale gas in China. Petroleum Exploration and Development, 2010, 37(6): 641-653.

Zou, C., Zhao, Q., Li, J., et al. Principal characteristics of marine shale gas and theory and technology of its exploration and development in China. Natural Gas Industry B, 2023, 10(1): 1-13.